Journal of Coordination Chemistry

Spectral, thermal, electrochemical, biological and DFT studies on nanocrystalline Co(II), Ni(II), Cu(II) and Zn(II) complexes with a tridentate ONO donor Schiff base ligand

Chellaian Justin Dhanaraj & Jijo Johnson

Taylor & Francis
Taylor & Francis Group

Spectral, thermal, electrochemical, biological and DFT studies on nanocrystalline Co(II), Ni(II), Cu(II) and Zn(II) complexes with a tridentate ONO donor Schiff base ligand

CHELLAIAN JUSTIN DHANARAJ* and JIJO JOHNSON

Department of Chemistry, University College of Engineering, Anna University Constituent College, Nagercoil, India
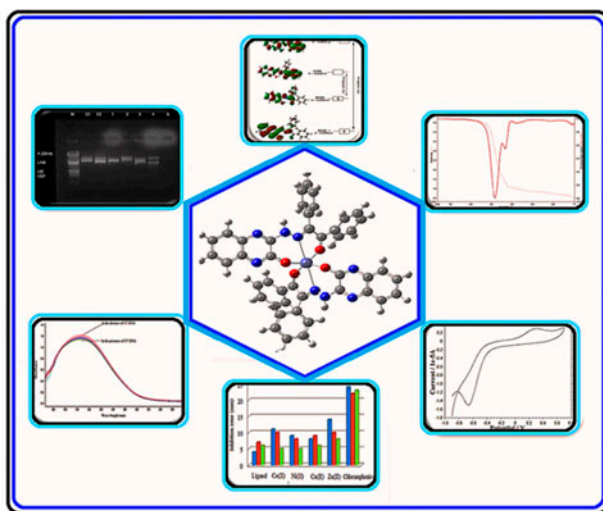
Co(II), Ni(II), Cu(II) and Zn(II) Schiff base complexes derived from 3-hydrazinoquionoxaline-2-one and 1,2-diphenylethane-1,2-dione were synthesized. The compounds were characterized by elemental analyses, molar conductance, magnetic susceptibility measurements, FTIR, UV–vis, ^{1}H NMR, ^{13}C NMR, ESR, and mass spectral studies. Thermal studies of the ligand and its metal complexes were also carried out to determine their thermal stability. Octahedral geometry has been assigned for Co(II), Ni(II), and Zn(II) complexes, while Cu(II) complex has distorted octahedral geometry. Powder XRD study was carried out to determine the grain size of ligand and its metal complexes. The electrochemical behavior of the synthesized compounds was investigated by cyclic voltammetry. For all complexes, a 2 : 1 ligand-to-metal ratio is observed. The ligand and its metal complexes were screened for their activity against bacterial species such as *E. coli*, *P. aeruginosa,* and *S. aureus* and fungal species such as *A. niger*, *C. albicans,* and *A. flavus* by disk diffusion method. The DNA-binding of the ligand and its metal complexes were investigated by electronic absorption titration and viscosity measurement studies. Agarose gel electrophoresis was employed to determine the

---

*Corresponding author. Email: c.justindhanaraj@gmail.com

DNA-cleavage activity of the synthesized compounds. Density functional theory was used to optimize the structure of the ligand and its Zn(II) complex.

Keywords: Thermal studies; Electrochemical; XRD; DNA; DFT

1. Introduction

Schiff base ligands have high coordination capability and can be easily synthesized by condensation of primary amines and carbonyl compounds [1]. The azomethine or imino group has good donor properties and can form stable complexes with transition metal ions [2, 3]. Schiff bases containing heterocyclic moieties have interesting properties due to their diverse anticancer, antiviral, fungicidal, bactericidal, and anti-HIV activities [4]. The positively charged metal centers are preferential to bind with negatively charged biomolecules such as the amino acid residues of protein constituents, ATP, and nucleic acids [5]. Studies of the interaction of transition metal complexes with DNA have been an active subject in bioinorganic chemistry [6]. The interaction of DNA with transition metal complexes has been of interest because of its possible application in molecular biology and cancer therapy. Coordination compounds showed the unique chemical and physical properties as well as the abilities of their ligands to be adjusted to DNA interaction activities [7]. Literature survey revealed that studies on the synthesis of quinoxaline-based Schiff base complexes have importance because of their interesting chemical and biological properties [8]. Quinoxaline derivatives and their metal complexes have anti-bigram [9], cancer chemopreventive [10], cytotoxic [11], *in vitro* cyclooxygenase [12] and antimicrobial [13] activities. There is an increasing need for the synthesis of new compounds having antimicrobial, DNA-binding, DNA-cleaving and other activities.

In this study, we describe the synthesis and characterization of transition metal complexes of a tridentate (ONO donor) ligand having the quinoxaline ring system. In addition to analytical, spectral, thermal, and electrochemical studies, the complexes have been tested *in vitro* to assess their antimicrobial activities against bacterial and fungal species, and the results were compared with standards. We have carried out the DNA-binding and DNA-cleaving activities of the synthesized compounds against CT DNA and pUC18 DNA, respectively. The structural optimization and Density functional theory (DFT) studies of the ligand and one of its representative complexes are also discussed.

2. Experimental

2.1. *Materials*

The chemicals used were of AnalaR or synthetic grade; o-phenylenediamine was purchased from Loba Chemie, India. Oxalic acid, hydrazine hydrate, and metal(II) acetates were obtained from Merck and used as received.

2.2. *Instruments*

Elemental analysis of the ligand and its metal complexes were carried out using a Perkin-Elmer elemental analyzer. Molar conductances of the complexes were measured using a

coronation digital conductivity meter. IR spectra were recorded using a Jasco FTIR–4100 spectrometer in KBr pellets from 4000 to 400 cm^{-1}. ^{1}H NMR and ^{13}C NMR spectra were recorded with a Bruker 300 MHz spectrometer using CDCl$_3$ for ligand and its Zn(II) complex with TMS as internal standard. DART-MS spectra were recorded on a JEOL-Accu TOF JMS mass spectrometer. Magnetic moments were measured by the Guoy method and were corrected for diamagnetism of the component using Pascal's constants. Electronic spectra were recorded with a Thermo Scientific Evolution-200 UV–visible spectrophotometer from 190 to 1100 nm. ESR spectra of the Cu(II) complex were recorded at 300 and 77 K in DMSO solution with a Varian, USA E-112 ESR spectrometer using tetracyanoethylene (TCNE) as g-marker. Thermal analysis was carried out under nitrogen at a heating rate of 10 °C min^{-1} using a Perkin Elmer Diamond TG/DTA analyzer. Cyclic voltammetry measurements were performed with an electrochemical analyzer CH instruments electrochemical workstation (Model 650 C) using a glassy carbon working electrode (GCE), a Ag/AgCl reference electrode, and a platinum counter electrode. Powder XRD studies were carried out with a Bruker AXS D8 Advance X-ray diffractometer.

2.3. Synthesis of ligand

The ligand was synthesized by the following method. To a hot methanolic solution of 3-hydrazinoquinoxaline-2-one (2 mmol), methanolic solution of 1,2-diphenylethane-1,2-dione (2 mmol) was added dropwise with constant stirring at room temperature (scheme 1). To the above solution, few drops of concentrated H$_2$SO$_4$ were added. The mixture was then refluxed for 4–5 h, and the solid formed was filtered, washed with ether, and dried in vacuum over anhydrous calcium chloride.

2.4. Synthesis of metal complexes

Methanolic solution of metal(II) chlorides (2 mmol) was added to a methanolic solution of ligand (4 mmol), and the mixture was refluxed on a water bath for 5–6 h. The solid complexes obtained were filtered, washed with hot methanol, and dried in vacuum over anhydrous calcium chloride.

2.5. Biological studies

2.5.1. Antimicrobial and antifungal activity
In vitro antibacterial and antifungal activities of the ligand and its complexes were tested against the bacterial species *S. aureus*, *E. coli*,
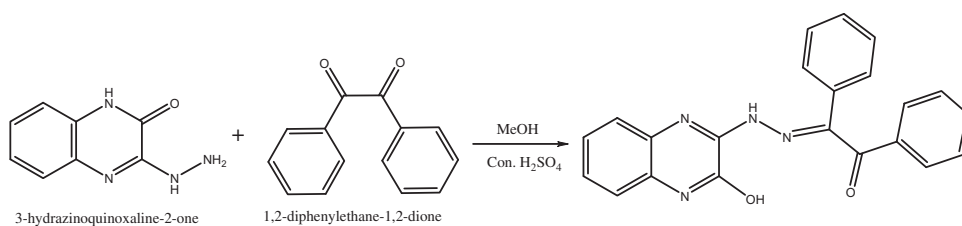
Scheme 1.   Synthetic route of the ligand.

and *P. aeruginosa* and the fungal species *C. albicans*, *A. flavus,* and *A. niger* by disk diffusion method [14]. Chloramphenicol and nystatin were used as standard antibacterial and antifungal agents, respectively. The test organisms were grown on nutrient agar (Muller Hinton agar for bacteria and antimytotic agar for fungi) medium in petri plates. The compounds were dissolved in DMF and soaked in a filter paper disk of 5 mm diameter and 1 mm thickness. The disks were placed on previously seeded plates and incubated at 37 °C. The diameter of inhibition zone around each disk was measured after 24 h for bacterial and 72 h for fungal species.

2.5.2. DNA-binding experiment

2.5.2.1. *Electronic absorption spectral studies.* A solution of CT DNA in the buffer (5 mM Tris–HCl/50 mM NaCl buffer (pH 7.2)) gave a UV absorbance ratio at 260 and 280 nm of about 1.89, indicating that the CT DNA was free from protein contamination. The CT DNA concentration was determined by UV absorption spectroscopy using the molar absorption coefficient of 6600 M^{-1} cm^{-1} at 260 nm. The stock solutions were kept at 4 °C and used within four days of preparation.

   Electronic absorption titrations were performed in Tris–HCl/NaCl buffer (5 mM Tris–HCl/50 mM NaCl buffer pH 7.2) using DMF (10%) solution of metal complexes at room temperature. Absorption titration experiments were made using different concentrations of CT DNA, keeping the complex concentration constant. Correction was made for absorbance of the CT DNA itself. Metal complex-DNA solutions were allowed to incubate for 5 min before the absorption spectra were recorded. For metal(II) complexes, the intrinsic binding constant (K_b) was determined by monitoring the changes of absorption in the MLCT band with the increase in concentration of DNA using the following equation [15]:

$$[DNA]/(\varepsilon_a - \varepsilon_f) = [DNA]/(\varepsilon_b - \varepsilon_f) + 1/K_b(\varepsilon_b - \varepsilon_f)$$

where [DNA] = concentration of DNA in base pairs, ε_a = apparent molar extinction coefficient, ε_f = molar extinction coefficient of free metal complex, and ε_b = molar extinction coefficient of the CT DNA bound-metal complex. A plot of [DNA]/($\varepsilon_b - \varepsilon_f$) *versus* [DNA] gave a slope of $1/(\varepsilon_b - \varepsilon_f)$ and a *y*-intercept equal to $K_b/(\varepsilon_b - \varepsilon_f)$; K_b is the ratio of the slope to the *y*-intercept.

2.5.2.2. *Viscosity measurements.* In order to confirm the binding modes of the compounds with CT DNA, viscosity measurements were carried out using an Ostwald viscometer maintained at room temperature (27 ± 1 °C). Flow time was measured three times with a digital stopwatch for each sample, and an average flow time was calculated. Data were presented as $(\eta/\eta_o)^{1/3}$ *versus* binding ratio. Relative viscosities for DNA were calculated using the relation, η/η_o,
where η = viscosity of CT DNA in the presence of complex and η_o = viscosity of CT DNA alone.

2.5.3. Cleavage of pUC18 DNA
The cleavage of supercoiled pUC18 DNA to its nicked circular form was studied using agarose gel electrophoresis. pUC18 DNA (0.3 μg) was dissolved in 5 mM Tris–HCl/50 mM NaCl buffer (pH 7.2) and was treated with the complexes. The mixture was incubated at 37 °C for 1 h and then mixed with the loading buffer containing 25% bromophenol blue,

0.25% xylene cyanol, and 30% glycerol. Each sample (10^{-3} mol, 0.5 μL) was loaded into 1% (w/v) agarose gel. Electrophoresis was undertaken for 2 h at 100 V in Tris–acetate–EDTA (TAE) buffer (pH 8.0). The gel was stained with ethidium bromide for 5 min after electrophoresis and then was photographed under a UV transilluminator. To improve the DNA-cleaving activity of the complexes, hydrogen peroxide (100 μM) was added to each sample [16]. The DNA-cleavage efficiency of the complexes was measured by determining the ability of the complexes to convert the supercoiled DNA into nicked circular form and linear form.

2.6. *DFT studies*

The geometrical optimization of the ligand and its Zn(II) complex was carried out theoretically by 6-31G(d,p) and B3LYP/LANL2DZ combinations, respectively, using Gaussian 09W [17] program package without any constraint. The geometry was optimized by DFT using Becker's three-parameter exchange functional (B3) [18] in combination with the Lee–Yang–Parr correlation functional (LYP) [19]. It was accepted as a cost-effective approach for the computation of molecular structure and energies of optimized structures. All computational processes of ligand were made using GaussView 5.0.8 [20]. Additionally, some quantum chemical parameters such as highest occupied molecular orbital (HOMO), lowest unoccupied molecular orbital (LUMO), HOMO–LUMO energy gap, Mulliken charges, natural bond orbital (NBO) charges, absolute electronegativity (χ_{abs}), absolute hardness (η), chemical potential (μ), electrophilicity index (ω), and global softness (S) were calculated. According to Kopmans' theorem [21],

$$-E_{\text{HOMO}} = \text{IE} \tag{1}$$

$$-E_{\text{LUMO}} = \text{EA} \tag{2}$$

where IE and EA are ionization energy and electron affinity, respectively. The absolute electronegativity (χ_{abs}) and absolute hardness (η) are related to IA and EA [22] as given below.

$$\chi_{abs} = (\text{IE} + \text{EA})/2 = (E_{\text{HOMO}} + E_{\text{LUMO}})/2 \tag{3}$$

$$\eta = (\text{IE} - \text{EA})/2 = (E_{\text{HOMO}} - E_{\text{LUMO}})/2 \tag{4}$$

Two other properties related to chemical potential (μ) [23] and hardness (η) are electrophilicity index (ω) and global softness (S) [24]. These values were calculated using equations (5)–(7).

$$\mu = -(E_{\text{HOMO}} + E_{\text{LUMO}})/2 \tag{5}$$

$$\omega = \mu^2/2\eta \tag{6}$$

$$\text{S} = 1/\eta \tag{7}$$

3. Results and discussion

The analytical data of prepared ligand and its Co(II), Ni(II), Cu(II), and Zn(II) complexes are given in table 1. All complexes are soluble in organic solvents such as DMF, DMSO, and CHCl₃, but insoluble in water. The ligand and its metal complexes are stable at room temperature in the solid state.

3.1. *Molar conductance*

Molar conductance measurement was performed in DMF (10^{-3} M) solutions at room temperature to establish the charge of the metal complexes. The molar conductance data (table 1) indicate that all metal complexes have low conductivity values in accordance with non-electrolytes [25].

3.2. *IR spectra*

From table 2, it is clear that IR spectra of the complexes differ slightly from the IR spectrum of free ligand. The spectrum of free ligand shows two strong bands at 1630 and 1678 cm^{-1} characteristic of the >C=N (imine) and >C=O (keto) stretching vibrations, respectively. These bands are shifted to lower frequencies in spectra of the metal complexes, indicating the involvement of imino nitrogen and keto oxygen in chelation with the metal ion [26]. The broad band at 3050 cm^{-1} in the IR spectrum of the ligand is assigned to phenolic –OH stretching vibrations of quinoxaline moiety. The low value of this band is due to intramolecular hydrogen bonding between the hydrogen of –OH group and the imine nitrogen (–OH⋯N=C<) [27]. This band is absent in all metal complexes, suggesting the involvement of –OH group in bond formation with metal ion in the metal complexes through deprotonation [28]. The IR spectrum of the ligand exhibits also a strong band at 1321 cm^{-1} ascertained to v(C–O) stretching vibration [29]. The shift of this band to lower frequencies supports M–O bond formation through deprotonation of phenolic oxygen. The presence of new bands in the spectra of all metal complexes in the low frequency regions 488–465 cm^{-1} and 689–647 cm^{-1} are characteristic of v(M–N) and v(M–O) stretches, respectively [30]. These bands are not observed in the spectrum of free ligand.

Table 1. Analytical data and physical data of the ligand and its metal complexes.

Compound	Yield (%)	M. Wt	Decomposition temperature (°C)	Elemental analysis (%) found (calculated)					Molar conductivity (Ω^{-1} cm^2 mol^{-1})
				C	H	N	O	M	
C₂₂H₁₆N₄O₂	88	369	160	71.69 (71.73)	4.43 (4.38)	15.43 (15.21)	8.45 (8.69)	–	–
C₄₄H₃₀N₈O₄Co	75	794	180	66.32 (66.58)	3.72 (3.81)	14.09 (14.12)	8.08 (8.06)	7.79 (7.43)	7.52
C₄₄H₃₀N₈O₄Ni	80	794	150	66.34 (66.60)	3.74 (3.81)	14.08 (14.12)	8.10 (8.06)	7.74 (7.40)	9.90
C₄₄H₃₀N₈O₄Cu	65	799	195	66.48 (66.20)	3.70 (3.79)	14.03 (14.04)	8.05 (8.02)	7.74 (7.96)	6.85
C₄₄H₃₀N₈O₄Zn	73	800	190	66.07 (66.05)	3.57 (3.78)	14.06 (14.00)	8.10 (8.00)	8.20 (8.17)	4.72

Table 2. IR spectral data of the ligand and its complexes (cm^{-1}).

Compound	v(NH)	v(OH)	v(C=N)	v(C=O)	v(C–O)	v(M–O)	v(M–N)
$C_{22}H_{16}N_4O_2$	3336	3050	1630	1678	1321	–	–
$C_{44}H_{30}N_8O_4Co$	3343	–	1622	1671	1318	648	488
$C_{44}H_{30}N_8O_4Ni$	3444	–	1621	1670	1318	689	484
$C_{44}H_{30}N_8O_4Cu$	3460	–	1623	1674	1317	647	474
$C_{44}H_{30}N_8O_4Zn$	3418	–	1620	1672	1315	638	465

Based on the IR spectral analysis of metal complexes, it is concluded that the ligand is tridentate in the complexes, coordinated through phenolic –OH, imino nitrogen, and >C=O group of 1,2-diphenylethane-1,2-dione (table 2).

3.3. ^{1}H- and ^{13}C NMR spectra

The ^{1}H- and ^{13}C NMR spectra of the free ligand and its Zn(II) complex were recorded in $CDCl_3$ solution using TMS as internal standard.

A singlet at 9.1 ppm has been assigned to free –NH proton [31], which remains unchanged in the spectrum of Zn(II) complex. This indicates non-involvement of –NH in coordination. The phenolic –OH proton has a resonance at 4.85 ppm [32], which is absent in the spectrum of Zn(II) complex revealing participation of phenolic –OH in chelation through deprotonation. The aromatic protons are observed at 7.2–8.0 ppm (figures S1 and S2, see online supplemental material at http://dx.doi.org/10.1080/00958972.2015.1051475) [33].

In the ^{13}C NMR spectrum (figure S3) of the ligand, the signals for the corresponding keto, imino, and aromatic carbons are present. The signals at 198.5 and 168 ppm are attributed to the keto and imino carbons, respectively. Other downfield signals at 128–137 ppm are assigned to the aromatic and quinoxaline ring carbons [34]. ^{13}C NMR spectrum of the Zn(II) complex (figure S4) shows small shifts of these peaks due to coordination of Zn(II). This further confirms the proposed structure of the complex.

3.4. Mass spectra

In the DART mass spectrum, the molecular ion peak of the ligand is noted at 369 *m/z*. The molecular ion peaks of the Co(II), Ni(II), Cu(II), and Zn(II) complexes are observed at 794, 794, 799, and 800 *m/z*, respectively. In addition, the spectra of the ligand and metal complexes show series of peaks corresponding to their various fragments. Elemental analysis values agree with the values calculated from the molecular formula assigned to these compounds which are further supported by mass spectral studies.

3.5. Electronic spectra

Electronic spectra of the compounds (table 3) were recorded in DMF at room temperature from 190 to 1100 nm. The electronic spectrum of the ligand exhibits two bands at 235–278 nm, assigned to intraligand π–π* transitions of the aromatic rings present in the ligand [35]. This remains almost unchanged in spectra of the complexes. The band at 314 nm is assigned to n–π* transitions of the imine (>C=N) and keto (>C=O) groups. In the metal complexes, this band is shifted, suggesting the coordination of imino nitrogen and oxygen.

Table 3. Electronic spectral and magnetic moment data of the metal(II) complexes.

Complex	λ_{max} (nm)	Band assignments	Magnetic moment (BM)	Geometry
$C_{44}H_{30}CoN_8O_4$	680	$^4T_{1g}$ (F) $\rightarrow$ $^4A_{2g}$ (F)	5.15	Octahedral
	588	$^4T_{1g}$ (F) $\rightarrow$ $^4T_{2g}$(P)		
	395	$^4T_{1g}$ (F) $\rightarrow$ $^4T_{1g}$ (P)		
$C_{44}H_{30}NiN_8O_4$	700	$^3A_{2g}$ (F) $\rightarrow$ $^3T_{1g}$ (F)	2.91	Octahedral
	400	$^3A_{2g}$(F) $\rightarrow$ $^3T_{1g}$ (P)		
$C_{44}H_{30}CuN_8O_4$	464	$^2B_{1g} \rightarrow {}^2B_{2g}$ π–π^*	1.98	Distorted octahedral
$C_{44}H_{30}ZnN_8O_4$	–	–	Diamagnetic	Octahedral

The spectrum of Co(II) complex shows three bands. Two bands at 680 and 588 nm are assigned to $^4T_{1g}$ (F) $\rightarrow$ $^4A_{2g}$ (F) and $^4T_{1g}$ (F) $\rightarrow$ $^4T_{2g}$ (P) transitions, respectively. The band at 395 nm is assigned to $^4T_{1g}$ (F) $\rightarrow$ $^4T_{1g}$ (P) transition for octahedral geometry. The Ni(II) complex shows two bands at ~700 and ~400 nm matching to octahedral geometry with the following transitions: $^3A_{2g}$ (F) $\rightarrow$ $^3T_{1g}$ (F) and $^3A_{2g}$ (F) $\rightarrow$ $^3T_{1g}$ (P). The electronic spectrum of the Cu(II) complex shows one band at 464 nm, assigned to $^2B_{1g} \rightarrow {}^2B_{2g}$ transition, indicating that the complex has distorted octahedral geometry [36]. The Zn(II) complex is expected to have octahedral geometry.

3.6. Magnetic measurements

Magnetic susceptibility measurements of the powdered complexes were carried out by employing Guoy's method at room temperature. Copper sulfate was used as calibrant. The effective magnetic moment, μ_{eff}, of the metal ions was calculated using the following formula,

$$\mu_{eff} = 2.83 \, (\chi_m T)^{1/2} \text{BM}$$

where χ_m = molar susceptibility and T = absolute temperature. The μ_{eff} of the metal ions was calculated after making proper diamagnetic [37] corrections using Pascal's constants.

The Co(II) complex has a magnetic moment of 5.15 BM, in agreement with the reported values for octahedral Co(II) complexes. The Ni(II) complex shows magnetic moment of 2.91 BM in the expected range of 2.9–3.3 BM, suggesting octahedral environment. The Cu(II) complex shows magnetic moment of 1.98 BM, higher than the spin-only value 1.73 BM, expected for one unpaired electron, monomeric and consistent with distorted octahedral geometry [38].

3.7. EPR spectroscopy

X-band EPR spectra of the Cu(II) complex recorded in DMSO at liquid nitrogen temperature (77 K) and at room temperature (300 K) are given in figure 1. The spin Hamiltonian parameters calculated are given in table 4. The EPR spectrum of the Cu(II) complex at room temperature shows a single isotropic broad signal in the high field due to tumbling motion of the molecules. The EPR spectrum of the Cu(II) complex at liquid nitrogen temperature shows four well-resolved peaks [39]. The $g_{\parallel} > g_{\perp} > 2.0027$ observed for the complex indicate that the unpaired electron is localized in the $d_{x^2-y^2}$ orbital of Cu(II). From the observed values, clearly $g_{\parallel} = 2.30 > g_{\perp} = 2.06 > 2.0027$ and the EPR parameters of the complex coincide well with related systems, which suggests that the complex has distorted octahedral geometry. This is also supported by the fact that the unpaired electron lies predominantly in the $d_{x^2-y^2}$ orbital.

The geometric parameter G, which is the measure of exchange interaction between the copper center in polycrystalline compounds, is calculated using the equation $G = (g_{\parallel} - 2.0027)/(g_{\perp} - 2.0027)$. According to Hathaway [40], if the value of G is greater than four, the exchange interaction between Cu(II) centers in the solid state is negligible, when it is less than four, a considerable exchange interaction is shown in the solid complex. The calculated G value (4.3) for the copper complex indicates that magnetic interaction between Cu(II) ions is negligible in the solid complex [41].

The EPR parameters $g_{\parallel}$, $g_{\perp}$, g_{av}, $A_{\parallel}$ and $A_{\perp}$ for the Cu(II) complex and the energies of d–d transitions were used to evaluate the bonding parameters α^2, β^2 and γ^2 which may be regarded as a measure of the covalency of the in-plane σ-bonding, in-plane π-bonding and out-of-plane π-bonding, respectively. The values were calculated using the expressions reported earlier [42] and are given in table 4.

According to Hathaway [43], for pure σ-bonding $K_{\parallel} \approx K_{\perp} \approx 0.77$ and for in-plane σ-bonding $K_{\parallel} < K_{\perp}$, while for out-of-plane π-bonding $K_{\perp} < K_{\parallel}$. Further α^2, β^2 and γ^2 values less than unity are expected for 100% ionic character of the bonds. In this study, the Cu(II) complex has $K_{\perp} < K_{\parallel}$ values indicating the presence of significant out-of-plane π-bonding. The observed α^2 (0.7284), β^2 (1.3278) and γ^2 (1.0237) values reveal that there is significant covalent bonding between the ligand and Cu(II). The results of EPR parameters, electronic absorption and magnetic measurement data reveal that the synthesized Cu(II) complex has distorted octahedral geometry with significant covalent bonding.

3.8. Thermal studies

Thermal stabilities of the ligand and its metal complexes were studied using TG and DTA under nitrogen with a heating rate of 10 °C min^{-1} from 40 to 700 °C. All the synthesized compounds show multistage decomposition pattern. The temperature at which a compound
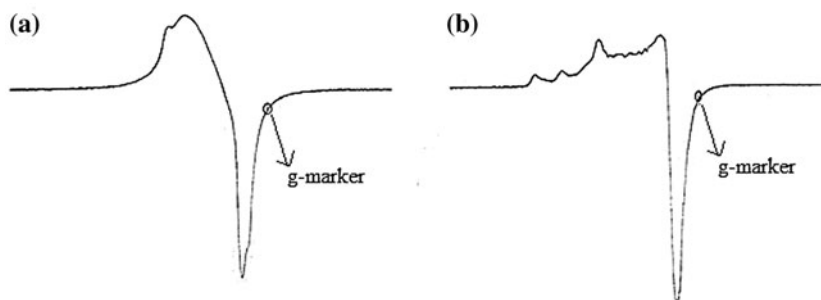

Figure 1. EPR spectra of the Cu(II) complex at (a) room temperature and (b) liquid nitrogen temperature.

Table 4. Spin Hamiltonian parameters of the Cu(II) complex in DMSO.

Complex	g tensors			Hyperfine constant $\times 10^{-4}$			Bonding parameters					
	$g_{\parallel}$	$g_{\perp}$	g_{av}	$A_{\parallel}$	$A_{\perp}$	A_{av}	G	α^2	β^2	γ^2	$K_{\parallel}$	$K_{\perp}$
$C_{44}H_{30}CuN_8O_4$	2.30	2.06	2.18	132	90	111	4.3	0.7284	1.3278	1.0237	0.9671	0.7456

starts its decomposition is represented by T_d [44]. T_d for ligand, Co(II), Ni(II), Cu(II), and Zn(II) complexes are 160, 180, 150, 195, and 190 °C, respectively. The ligand exhibits three stages of decomposition (figure S5), 160–195 °C, 195–265 °C, and 265–440 °C, with endothermic DTA peaks at 178, 238, and 320 °C, respectively. The Co(II) complex shows three stages of decomposition (figure S6). The first stage decomposition occurs at 180–320 °C. In DTA, an endothermic peak is at 311 °C. The second stage decomposition occurs at 320–355 °C with an endotherm in DTA at 351 °C; these two stages of decompositions correspond to degradation of ligand moiety. The final stage decomposition (355–440 °C) occurs with endotherm at 415 °C. After 415 °C, no decomposition occurs which may be due to the formation of metal oxide residue in the third stage.

The Ni(II) and Zn(II) complexes show two stages of thermal decomposition. For Ni(II) complex (figure S7), the first stage of thermal degradation starts at 150 °C and ends at 345 °C. The second stage decomposition is from 345 to 515 °C. These two stages of decomposition with endothermic DTA peaks at 310 and 418 °C are due to the decomposition of ligand and metal oxide moieties, respectively. The Zn(II) complex exhibits two stages of decomposition (figure S9) at 190–345 °C and 345–395 °C with endothermic DTA peaks at 317 and 368 °C, respectively. The Cu(II) complex shows three stages of thermal decomposition (figure S8). The first-stage thermal decomposition (195–340 °C) with an endotherm at 312 °C is due to loss of organic moieties from the metal complex. The other two stages of degradation occur at 340–395 °C and 470–560 °C with corresponding endothermic peaks at 384 and 516 °C, respectively. Thermal analysis results are in agreement with the formulas of the complexes from analytical data. From the T_d values of all compounds, it can be recognized that the Cu(II) complex has high thermal stability and the Ni(II) complex has the least thermal stability. The order of stability varies in the following order: Cu(II) > Zn(II) > Co(II) > Ligand > Ni(II).
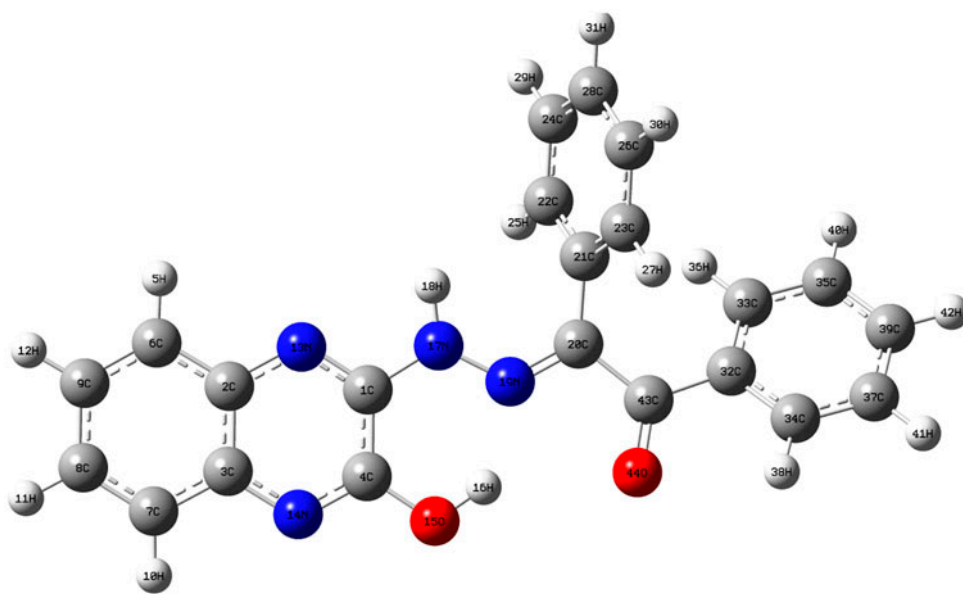

Figure 2.   Optimized geometry of the ligand (gray balls – C, white balls – H, blue balls – N and red balls – O) (see http://dx.doi.org/10.1080/00958972.2015.1051475 for color version).
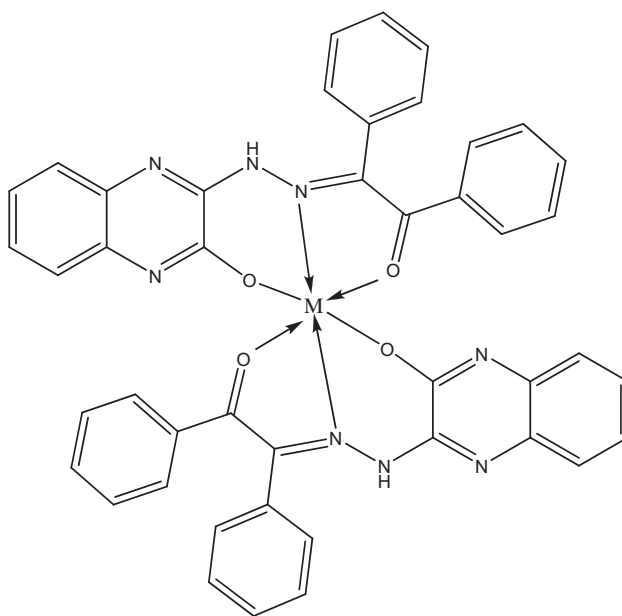
Figure 3. Proposed structure of the metal complexes [M = Co(II), Ni(II), Cu(II) and Zn(II)].

Based on the above results, the optimized structure of the ligand and proposed structure of metal complexes are given in figures 2 and 3, respectively.

3.9. *Electrochemical studies*

The cyclic voltammograms of the compounds were recorded at 300 K in DMSO solution within with scan rate 0.05 V s^{-1}. The potential range was −1.0 to 0.6 V for ligand and its Co(II) and Ni(II) complexes. The potential range for Cu(II) and Zn(II) complexes was −1.0 to 0.8 V. The cyclic voltammetric data of the compounds (figure S10) are summarized in table 5. A comparison of cyclic voltammetric data of the ligand with its metal complexes gives information about the redox reaction of the metal complexes, viz. whether the redox reaction is metal-centered or ligand-centered.

The ligand shows one irreversible couple with E_{pc} = −0.3 V *versus* Ag/AgCl and the associated anode peak at E_{pa} = −0.67 V. The large separation ΔE = 0.97 V indicates irreversible couple. The Co(II) complex shows redox process corresponding to formation of the quasi-reversible Co(II)/Co(I) couple. The anodic peak is observed at E_{pa} = −0.57 V *versus* Ag/AgCl, and the associated cathodic peak at E_{pc} = −0.72 V. The peak-to-peak separation, ΔE_{p} for this quasi-reversible process is 0.15 V. The Ni(II) complex shows two quasi-reversible peaks at E_{pa} = −0.70 V and E_{pc} = −0.59 V corresponding to Ni(II)/Ni(I) couple. The peak-to-peak separation, ΔE_{p}, is 0.11 V. The Cu(II) complex shows quasi-reversible cathodic peak at E_{pc} = 0.425 V *versus* Ag/AgCl corresponding to Cu(II)/Cu(III) couple, and the associated anodic peak at E_{pa} = 0.025 V. The ΔE_{p} is 0.40 V, confirming that the process is quasi-reversible. The Zn(II) complex shows an irreversible cathodic peak at 0.30 V *versus* Ag/AgCl, and the associated anodic peak at E_{pa} = −0.64 V. The peak-to-peak separation,

Table 5.   Cyclic voltammetric data of the ligand and its complexes.

Complex	E_{pc} (V)	E_{pa} (V)	ΔE_p (V)	I_{pc}/I_{pa}
$C_{22}H_{16}N_4O_2$	0.30	−0.67	0.97	0.72
$C_{44}H_{30}N_8O_4Co$	−0.72	−0.57	0.15	0.16
$C_{44}H_{30}N_8O_4Ni$	−0.59	−0.70	0.11	0.52
$C_{44}H_{30}N_8O_4Cu$	0.425	0.025	0.44	0.84
$C_{44}H_{30}N_8O_4Zn$	0.30	−0.64	0.94	0.14

ΔE, is 0.94 V. On comparing the electrochemical parameters of the ligand and Zn(II) complex, it is clear that the redox behavior of Zn(II) complex is purely ligand-based.

The electrochemical analysis of the complexes reveals that all complexes except Zn(II) exhibit quasi-reversible redox processes. The separation between cathodic and anodic peak potentials (ΔE) for the redox couples is greater than 0.06 V, and the values of peak current ratio (I_{pc}/I_{pa}) are not unity [45].

3.10. Powder XRD

Powder XRD patterns of the ligand and its complexes were recorded at $2\theta = 0–80°$ and are given in figures S11–S15. The 2θ, interplanar spacing d (Å), and intensity values are given as Supplementary Data. All compounds display well-defined crystalline peaks indicating the complexes as crystalline. The d-spacing values are different for the ligand and its complexes and are attributed to the formation of metal complexes. From the observed d_{XRD} patterns, the grain size of the ligand and its complexes were calculated from Schererr's formula [46], $d_{XRD} = 0.9\lambda/\beta Cos\theta$, where d_{XRD} is the particle size, λ is the wavelength of X-ray radiation, β is the full-width half maximum, and θ is the diffraction angle for the hkl plane. From the observed d_{XRD} patterns, the average crystallite sizes of the ligand, Co(II), Ni(II), Cu(II), and Zn(II) complexes are 8.64, 12.03, 10.66, 7.00, and 08.98 nm, respectively, suggesting that the compounds are in nanocrystalline phase [47].

3.11. Biological studies

3.11.1. In vitro antimicrobial activity

The *in vitro* antimicrobial activity of the ligand and its complexes are presented in figures 4 (a) and 4(b). The standard error for the experiment is ±0.001 mm, and the experiment is repeated three times under similar conditions. DMF is used as negative control; chloramphenicol is used as positive standard for antibacterial and nystatin for antifungal activities.

In this study, the metal complexes possess higher antimicrobial activity than the ligand. The order of the antimicrobial activity of the synthesized compounds is the following:

$$Zn(II) > Co(II) > Cu(II) > Ni(II) > Ligand$$
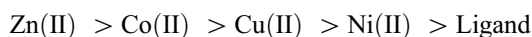
This high antimicrobial activity of the metal complexes may be due to the change in structure because of coordination and chelation which tend to make metal complexes more powerful bacteriostatic agents, thus inhibiting the growth of the microorganisms [48]. The lower activity of the Co(II), Cu(II), and Ni(II) complexes may be either due to
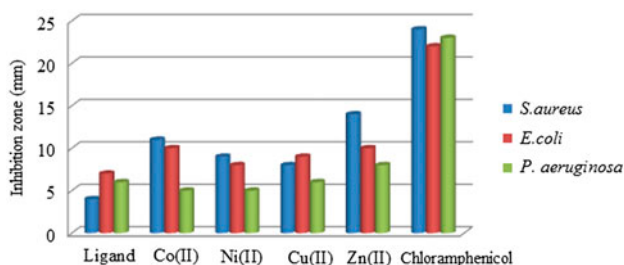
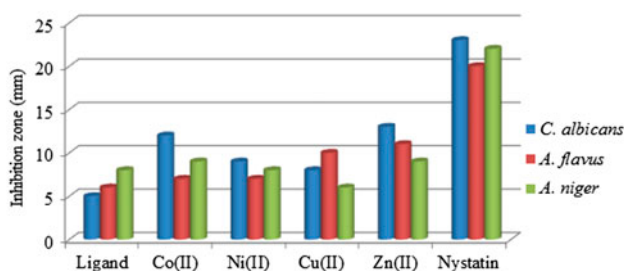Figure 4(a). Antibacterial activity of the ligand and its metal complexes.

Figure 4(b). Antifungal activity of the ligand and its metal complexes.

the inability of the complexes to diffuse into the bacterial cell membrane becoming unable to interfere with its biological activity, or they can diffuse and become inactivated by bacterial enzymes [49].

3.11.2. DNA-binding studies

3.11.2.1. *Electronic absorption spectral studies.* Electronic absorption spectrum of Cu(II) complex in the absence and presence of CT DNA is shown in figure 5. The Co(II) complex shows a band at 321.92 nm. On increasing the CT DNA concentration, absorption intensity decreased (hypochromism) and wavelength increased slightly to 322.40 nm (bathochromism). Similarly, the ligand and its Ni(II), Cu(II), and Zn(II) complexes exhibit also hypochromism and bathochromism, and the results are given in table 6.

In general, hypochromism associated with bathochromism represents intercalative mode of interaction. In intercalation, the metal complexes bind with CT DNA through a strong interaction of aromatic chromophores of the complex with the base pairs of DNA [50]. To measure the extent of intercalation, the intrinsic binding constant (K_b) values of the metal complexes are determined (table 6) by plotting [DNA] *versus* [DNA]/($\varepsilon_a - \varepsilon_f$) (figure 5). The K_b values obtained in this study indicate that the ligand and its metal complexes are moderate intercalators. Among the compounds, Zn(II) complex and ligand show higher and lower, respectively, binding affinities toward CT DNA.

3.11.2.2. *Viscosity measurements.* Optical or photophysical probes generally provide necessary but not sufficient clues to support an intercalative binding model. Therefore, the
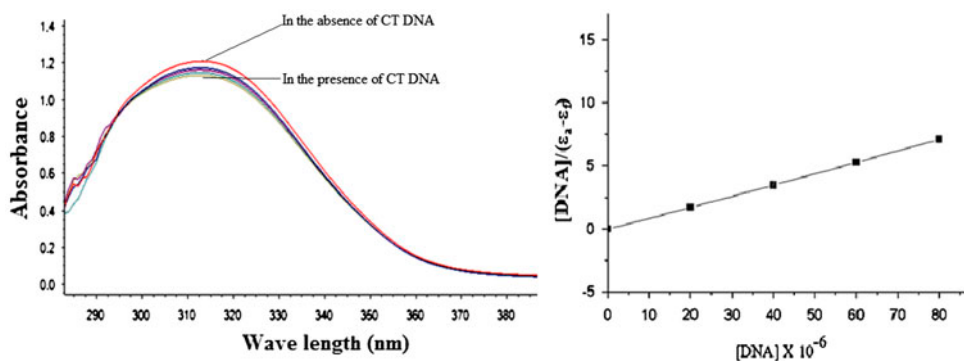
Figure 5.　Electronic absorption spectra of Cu(II) complex in the presence and absence of CT DNA.

Table 6.　Electronic absorption spectral properties of the ligand and its metal complexes.

| Complex | λ_{max} (nm) | | $\Delta\lambda$ (nm) | Hypochromicity (%) | K_b ($\times 10^4$) M^{-1} |
	Free	Bound			
$C_{22}H_{16}N_4O_2$	314. 57	315.02	0.45	10.50	3.9
$C_{44}H_{30}N_8O_4Co$	321.92	322.40	0.48	11.40	4.3
$C_{44}H_{30}N_8O_4Ni$	318.94	319.72	0.78	17.90	4.5
$C_{44}H_{30}N_8O_4Cu$	312.73	313.31	0.58	13.30	4.2
$C_{44}H_{30}N_8O_4Zn$	312.26	314.13	1.87	22.70	6.3

hydrodynamic method is regarded as one of the least ambiguous and most critical tests of a binding in solution in the absence of crystallographic structural data [51]. Since viscosity of DNA is sensitive to its length, it is expected that the intercalating agents will elongate the double helix and lead to an increase in the viscosity of DNA. Partial or non-classical inter-calation of compounds could bend or kink the DNA helix reducing the effective length of DNA, and subsequently, the viscosity decreases [39]. Viscosity measurements were per-formed by varying the concentration of the compounds with constant DNA concentration. The effects of metal complexes on the viscosities of CT DNA are shown in figure 6. The relative viscosity of DNA increased steadily on increasing the concentration of the synthe-sized compounds. This indicates the occurrence of intercalation between the compounds and DNA. The DNA-binding affinity of the compounds is in the following order: Zn(II) > Ni(II) > Co(II) > Cu(II) > Ligand. These results are inconsistent with those obtained from electronic absorption spectral studies.

3.11.3.　Cleavage of pUC18 DNA
The DNA-cleavage activity of the ligand and its metal complexes with supercoiled pUC18 DNA was monitored by agarose gel electrophoresis in the presence of H_2O_2 as an oxidant. The DNA-cleavage activity of the compounds is shown in figure 7. Control experiments using only H_2O_2 did not show any significant DNA-cleavage under similar experimental conditions (lanes C1 and C2). The ligand and Ni(II) complexes cleave form-II of DNA, whereas Co(II) complex displays upward displacement of both forms of pUC18 DNA.
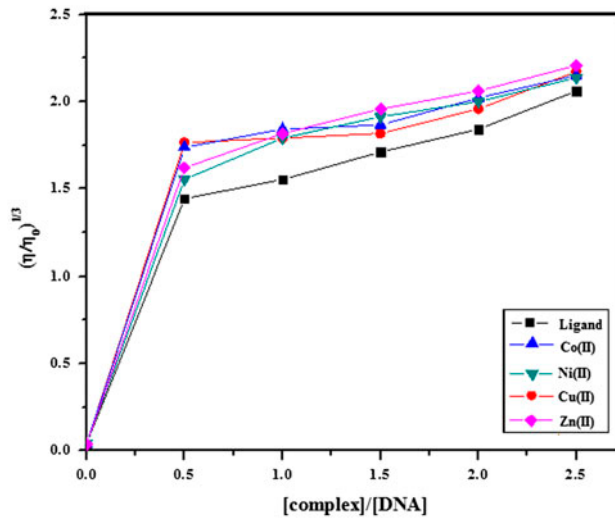
Figure 6. Effect of increasing amounts of the ligand and its Co(II), Ni(II), Cu(II), and Zn(II) metal complexes on relative viscosity of CT DNA.
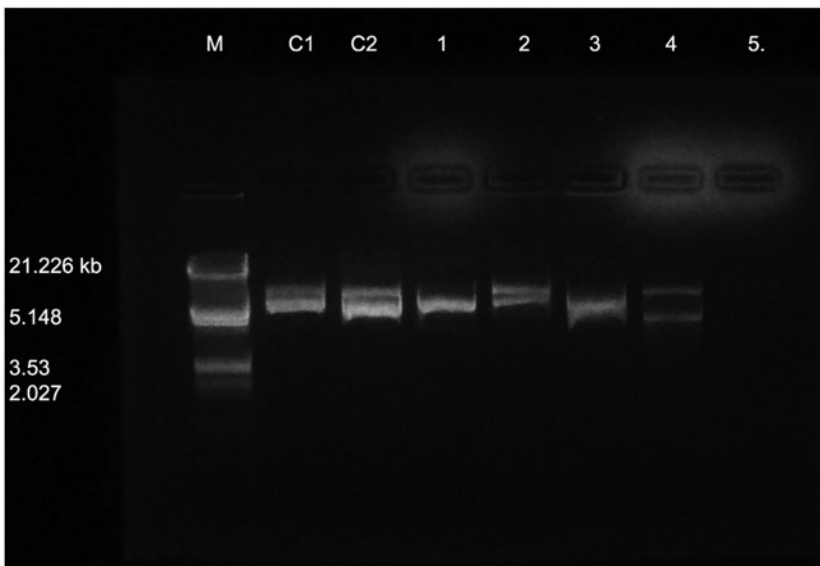

Figure 7. DNA-cleavage activity of the ligand and its metal complexes [M – Standard DNA molecular weight marker (λ DNA ECoRI/HindIII double digest, Merck, Bangalore); C1 – Control DNA (untreated sample); C2 – DNA treated with 100 μM H_2O_2. Lanes 1, 2, 3, 4, and 5 are DNA treated with ligand, Co(II), Ni(II), Cu(II), and Zn(II) complexes along with 100 μM H_2O_2].

An interesting significant separation of both forms of DNA was found with the Cu(II) complex. This was found because of downward displacement of form-I of DNA. In this study, the Zn(II) complex completely cleaves both forms of DNA. From the results, it is clear that the synthesized compounds have significant DNA-cleaving ability in the presence of an oxidizing agent.

3.12. *DFT studies*

The structure of the ligand and its Zn(II) complexes was optimized using B3LYP/6-31G(d,p) and B3LYP/LANL2DZ basis sets, respectively. The selected geometrical parameters for ligand and Zn(II) complex are given in tables 7 and 8, respectively. The optimized structure of the ligand with labeling is given in figure 2.

The energies for second-highest occupied MO (HOMO − 1), the HOMO, the lowest unoccupied molecular orbital (LUMO), and the second-lowest occupied molecular orbital (LUMO + 1) were calculated for both the ligand and Zn(II) complex. The calculated energies of the [HOMO − 1], HOMO, LUMO, and [LUMO + 1] for the ligand are −0.33694, −0.2990, −0.22181, and −0.19845 a.u, respectively. The energy gaps between [HOMO–LUMO] and {[HOMO − 1]–[LUMO + 1]} are −0.07719 and −0.11513 a.u, respectively, for the ligand molecule. The [HOMO − 1], HOMO, LUMO, and [LUMO + 1] energies and energy gaps between [HOMO–LUMO] and {[HOMO − 1]–[LUMO + 1]} are −0.26507, −0.23908, 0.00211, 0.02591, −0.24119, and −0.29098 a.u, respectively, for the Zn(II) complex.

Table 7.   Selected geometrical parameters of the ligand.

Bond connectivity	Bond length	Bond connectivity	Bond angle	Bond connectivity	Dihedral angle
1(C)–4(C)	1.4536	4(C)–15(O)–16(H)	111.6871	13(N)–1(C)–4(C)–14(N)	0.7515
1(C)–13(N)	1.3200	3(C)–14(N)–4(C)	119.2594	19(N)–20(C)–43(C)–32(C)	160.8761
4(C)–14(N)	1.3177	14(N)–4(C)–15(O)	117.5426	14(N)–4(C)–15(O)–16(H)	−179.9888
4(C)–15(O)	1.3578	4(C)–1(C)–13(N)	122.3225	13(N)–1(C)–17(N)–18(C)	4.0129
15(O)–16(H)	0.9986	13(N)–1(C)–17(N)	114.9683	1(C)–17(N)–19(N)–20(C)	−178.2325
1 (C)–17(N)	1.3994	1(C)–17(N)–18(H)	116.2916	19(N)–20(C)–43(C)–44(O)	−19.0056
17(N)–18(H)	1.0183	18(H)–17(N)–19(N)	122.8047	13(N)–1(C)–14(N)–15(O)	−178.7668
17(N)–19(N)	1.3400	17(N)–19(N)–20(C)	123.7288	4(C)–1(C)–13(N)–2(C)	−0.3188
19(C)–20(N)	1.3112	19(N)–20(C)–43(C)	112.3534	13(N)–1(C)–17(N)–19(N)	−177.3391
43(C)–44(O)	1.2536	20(C)–43(C)–44(O)	118.9625	33(C)–32(C)–43(C)–44(O)	153.8523

Table 8.   Selected geometrical parameters of the Zn(II) complex.

Bond connectivity	Bond length	Bond connectivity	Bond angle
87(Zn)–43(O)	2.0926	43(O)–87(Zn)–18(N)	65.475
87(Zn)–18(N)	2.5931	43(O)–87(Zn)–15(O)	92.611
87(Zn)–15(O)	1.9265	43(0)–87(Zn)–61(N)	113.277
87(Zn)–64(O)	2.0965	43(O)–87(Zn)–56(O)	96.618
87(Zn)–)–61(N)	2.7365	87(Zn)–61(N)–59(N)	120.265
87(Zn)–56(O)	1.9091	87(Zn)–64(O)–63(C)	130.580
19(C)–18(N)	1.2894	87(Zn)–18(N)–16(N)	123.472
18(N)–16(N)	1.3212	87(Zn)–56(O)–47(C)	149.553
42(C)–43(O)	1.2431	87(Zn)–43(O)–42(C)	128.626
56(O)–47(C)	1.2952	15(O)–4(C)–14(N)	122.987

Table 9.   Absolute electronegativity (χ_{abs}), absolute hardness (η), chemical potential (μ), electrophilicity index (ω), global softness (S), and dipole moment value for the ligand and its Zn(II) complex.

Parameters (eV)	B3LYP/6-31G(d,p) (ligand)	B3LYP/LANL2DZ (Zn(II) complex)
Absolute electronegativity	−0.26040	−0.11849
Absolute hardness	−0.03859	−0.120595
Chemical potential	0.26040	0.11849
Electrophilicity index	−0.87857	−8.46569
Global softness	−25.913	−8.29222

LUMO +1
E = -0.18945 a.u

LUMO
E = -0.22181 a.u

HOMO
E = -0.29900 a.u

HOMO - 1
E = -0.33694 a.u

$\Delta E = 0.07719$ a.u
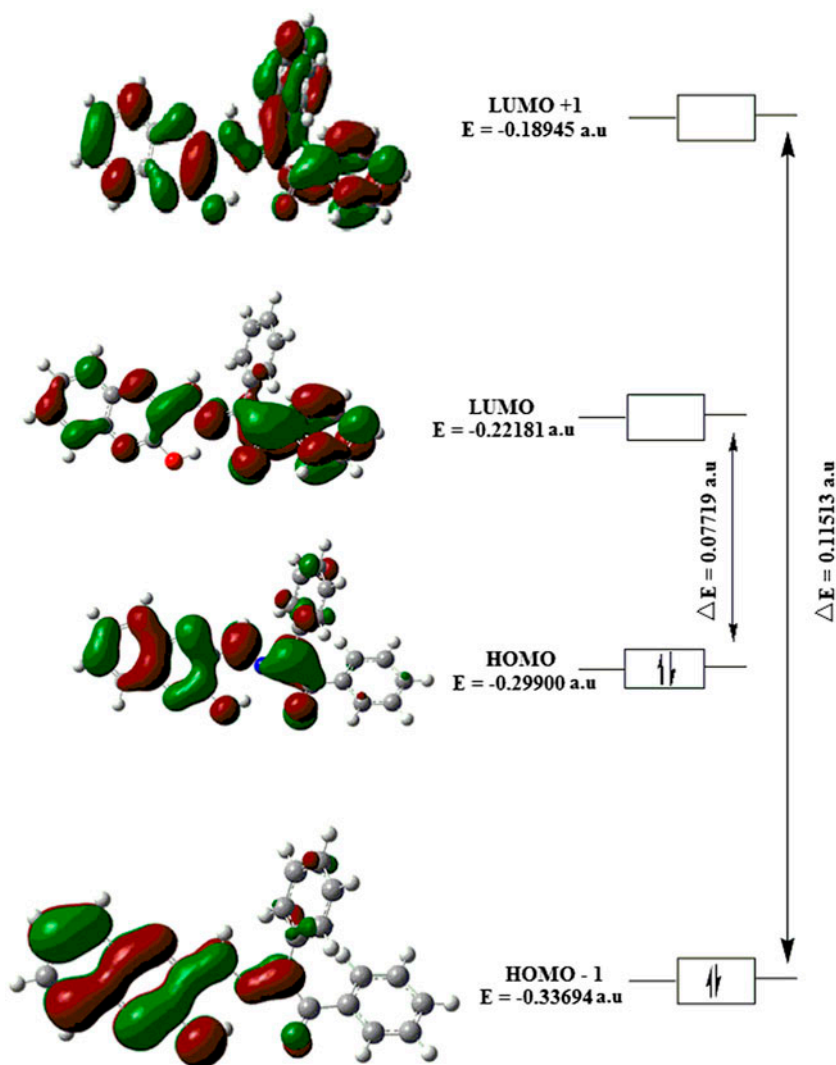
$\Delta E = 0.11513$ a.u

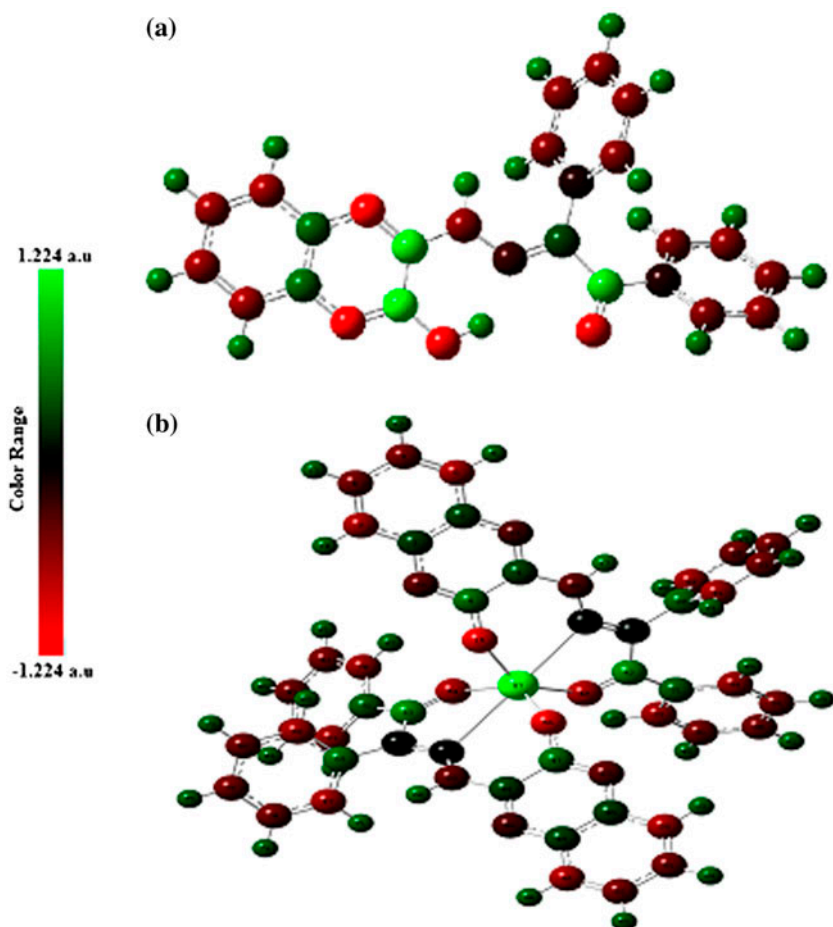Figure 8.   HOMO–LUMO structure with energy-level diagram of the ligand.

Figure 9.   Mulliken atomic charge distribution of the (a) ligand and (b) Zn(II) complex.

The HOMO–LUMO gap increases from soft to hard molecules [52]. The kinetic stability and reactivity pattern of a molecule can be ascertained from the HOMO–LUMO energy separation. If the HOMO–LUMO gap is small, it indicates low kinetic stability and high chemical reactivity since it is favorable energetically to add electrons to the LUMO or to extract electrons from the HOMO. Here, the metal complex has lower HOMO–LUMO energy gap and is more reactive than the corresponding ligand. As pointed out by Pearson [53], the chemical hardness of a molecule can be known from HOMO and LUMO energy separation. This in turn predicts their stability and reactivity. The hardness is directly proportional to the stability. Absolute electronegativity (χ_{abs}), absolute hardness (η), electrophilicity index (ω), and global softness (S) values are calculated using equations (1)–(6) given in the Experimental section and are displayed in table 9.

The HOMO–LUMO structures with energy-level diagram of the ligand are shown in figure 8. From the figure, one can say that the HOMO is concentrated on the quinoxaline
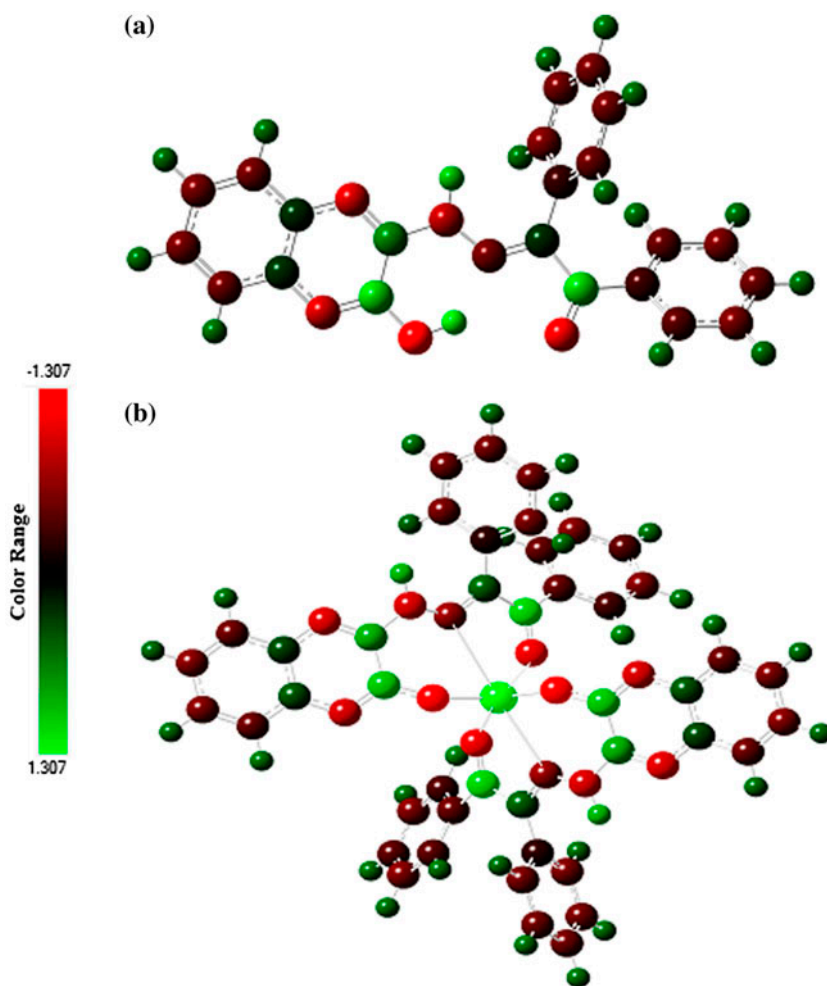
Figure 10.   NBO atomic charge distribution of the (a) ligand and (b) Zn(II) complex.

ring, imine >C=N bond, phenolic and carbonyl oxygens. Thus, they act as electron donors in metal chelates. The LUMO is mainly concentrated on the phenyl ring of benzil.

The atomic charges of ligand and its Zn(II) complex were obtained from Mulliken and natural atomic charge analysis with B3LYP/6-31G(d,p) and B3LYP/LANL2DZ basis sets, respectively, and are given in tables S1 and S2. The results show slight difference between Mulliken and natural atomic charges. From the atomic charge analysis, it is clear that C(8), C(9), N(13), C(24), C(28), C(37), C(39), and O(44) have negative charge in both Mulliken and NBO atomic charge analysis, whereas H(10), H(11), H(12), H(16), H(38), H(40), and H(41) have negative charge in Mulliken atomic charge analysis. C(6), C(7), N(14), N(15), N(17), N(15), N(17), C(21), C(22), C(23), C(26), C(32), C(33), C(34), and C(35) have negative charge in natural atomic charge analysis. The Mulliken and natural atomic charges of the ligand and Zn(II) complex are shown in figures 9(a,b) and 10(a,b), respectively.

4. Conclusion

Co(II), Ni(II), Cu(II), and Zn(II) Schiff base complexes derived from 3-hydrazinoquionoxaline-2-one and 1,2-diphenylethane-1,2-dione were synthesized. Octahedral geometry has been assigned for Co(II), Ni(II), and Zn(II) complexes. Cu(II) complex has distorted octahedral geometry. For all complexes, a 2 : 1 ligand-to-metal ratio is observed. The thermal studies indicate that the metal complexes are thermally more stable than the ligand. Powder XRD studies reveal that the metal complexes are nanocrystalline. Antimicrobial studies indicate that metal chelates have higher activity than the ligand. DNA-binding studies using electronic absorption titration and viscosity methods prove that the complexes exhibit DNA-binding through intercalation. DNA-cleavage activity of the synthesized compounds was investigated by agarose gel electrophoretic assay, and the complexes exhibit effective DNA-cleavage. We have optimized the structure of the ligand and its Zn(II) complex by DFT method. HOMO, LUMO, HOMO–LUMO gap, Mulliken charges, natural atomic charges, absolute electronegativity, absolute hardness, electrophilicity index, and global softness were calculated.

Disclosure statement

No potential conflict of interest was reported by the authors.

References

[1] M. Köse, G. Ceyhan, M. Tümer, İ. Demirtaş, İ. Gönül, V. McKee. *Spectrochim. Acta, Part A*, **137**, 477 (2015).
[2] A.A.S. Al-Hamdani, W. Al Zoubi. *Spectrochim. Acta, Part A*, **137**, 75 (2015).
[3] G.G. Mohamed, M.M. Omar, A.A. Ibrahim. *Spectrochim. Acta, Part A*, **75**, 678 (2010).
[4] N. Charef, F. Sebti, L. Arrar, M. Djarmouni, N. Boussoualim, A. Baghiani, S. Khennouf, A. Ourari, M.A. AlDamen, M.S. Mubarak, D.G. Peters. *Polyhedron*, **85**, 450 (2015).
[5] N. Raman, R. Mahalakshmi, T. Arun, S. Packianathan, R. Rajkumar. *J. Photochem. Photobiol. B*, **138**, 211 (2014).
[6] M. Gaber, H. El-Ghamry, F. Atlam, S. Fathalla. *Spectrochim. Acta, Part A*, **137**, 919 (2015).
[7] R. Gup, C. Gökçe, S. Aktürk. *Spectrochim. Acta, Part A*, **134**, 484 (2015).
[8] C.J. Dhanaraj, J. Johnson, J. Joseph, R.S. Joseyphus. *J. Coord. Chem.*, **66**, 1416 (2013).
[9] S. Budagumpi, N.V. Kulkarni, G.S. Kurdekar, M.P. Sathisha, V.K. Revankar. *Eur. J. Med. Chem.*, **45**, 455 (2010).
[10] S.A. Galal, A.S. Abdelsamie, H. Tokuda, N. Suzuki, A. Lida, M.M. ElHefnawi, R.A. Ramadan, M.H.E. Atta, H.I. El Diwani. *Eur. J. Med. Chem.*, **46**, 327 (2011).
[11] S.A. Galal, A.S. Abdelsamie, S.M. Soliman, J. Mortier, G. Wolber, M.M. Ali, H. Tokuda, N. Suzuki, A. Lida, R.A. Ramadan, H.I. El Diwani. *Eur. J. Med. Chem.*, **69**, 115 (2013).
[12] S.A. Galal, S.H.M. Khairat, F.A.F. Ragab, A.S. Abdelsamie, M.M. Ali, S.M. Soliman, J. Mortier, G. Wolber, H.I. El Diwani. *Eur. J. Med. Chem.*, **86**, 122 (2014).
[13] O.O. Ajani, C.A. Obafemi, O.C. Nwinyi, D.A. Akinpelu. *Bioorg. Med. Chem.*, **18**, 214 (2010).

[14] A.W. Bauer, W.M.M. Kirby, J.C. Sherries, M. Truck. *Am. J. Clin. Pathol.*, **45**, 493 (1966).

[15] C.J. Dhanaraj, J. Johnson. *Spectrochim. Acta, Part A*, **127**, 396 (2014).

[16] J. Sambrook, E.F. Fritsch, T. Maniatis. *Molecular Cloning, A Laboratory Manual*, 2nd Edn, Cold Spring Harbor Laboratory, Cold Spring Harbor, New York (1989).

[17] M.J. Frisch, G.W. Trucks, H.B. Schlegel, G.E. Scuseria, M.A. Robb, J.R. Cheeseman, G. Scalmani, V. Barone, B. Mennucci, G.A. Petersson, H. Nakatsuji, M. Caricato, X. Li, H.P. Hratchian, A.F. Izmaylov, J. Bloino, G. Zheng, J.L. Sonnenberg, M. Hada, M. Ehara, K. Toyota, R. Fukuda, J. Hasegawa, M. Ishida, T. Nakajima, Y. Honda, O. Kitao, H. Nakai, T. Vreven, J.A. Montgomery Jr., J.E. Peralta, F. Ogliaro, M. Bearpark, J.J. Heyd, E. Brothers, K.N. Kudin, V.N. Staroverov, T. Keith, R. Kobayashi, J. Normand, K. Raghavachari, A. Rendell, J.C. Burant, S.S. Iyengar, J. Tomasi, M. Cossi, N. Rega, J.M. Millam, M. Klene, J.E. Knox, J.B. Cross, V. Bakken, C. Adamo, J. Jaramillo, R. Gomperts, R.E. Stratmann, O. Yazyev, A.J. Austin, R. Cammi, C. Pomelli, J.W. Ochterski, R.L. Martin, K. Morokuma, V.G. Zakrzewski, G.A. Voth, P. Salvador, J.J. Dannenberg, S. Dapprich, A.D. Daniels, O. Farkas, J.B. Foresman, J.V. Ortiz, J. Cioslowski, D.J. Fox. *Gaussian 09, Revision D.01*, Gaussian Inc., Wallingford, CT (2013).

[18] A.D. Becke. *Phys. Rev. A*, **38**, 3098 (1988).

[19] C. Lee, W. Yang, R.G. Parr. *Phys. Rev. B*, **37**, 785 (1988).

[20] R. Dennington, T. Keith, J. Millam. *GaussView, Version 5*, Semichem Inc., Shawnee Mission, KS (2009).

[21] C.J. Brabec, N.S. Sariciftci, J.C. Hummelen. *Adv. Funct. Mater.*, **11**, 15 (2001).

[22] E. Ebenso, T. Arslan, F. Kandemirli, I. Love, C. Öğretır, M. Saracoğlu. *Int. J. Quantum Chem.*, **110**, 2614 (2010).

[23] P. Govindasamy, S. Gunasekaran. *J. Mol. Struct.*, **1081**, 96 (2015).

[24] R.C. Maurya, B.A. Malik, J.M. Mir, A.K. Sharma. *J. Coord. Chem.*, **67**, 3084 (2014).

[25] W.J. Geary. *Coord. Chem. Rev.*, **7**, 81 (1971).

[26] S.A. Patil, C.T. Prabhakara, B.M. Halasangi, S.S. Toragalmath, P.S. Badami. *Spectrochim. Acta, Part A*, **137**, 641 (2015).

[27] M. Sonmez, M. Sekerci. *Polish J. Chem.*, **76**, 907 (2002).

[28] M.A. Phaniband, S.D. Dhumwad, J.J. Jogul, P.G. Avaji. *Main Group Chem.*, **7**, 285 (2008).

[29] Z.H. Abd El-Wahab. *Spectrochim. Acta, Part A*, **67**, 25 (2007).

[30] K. Pothiraj, T. Baskaran, N. Raman. *J. Coord. Chem.*, **65**, 2110 (2012).

[31] G.S. Kurdekar, N.V. Kulkarni, S. Budagumpi, M.P. Sathisha, N.H. Bevinhalli, V.K. Revankar. *J. Coord. Chem.*, **63**, 2172 (2010).

[32] I. Sheikhshoaie, T. Shamspur, S. Yousef Ebrahimipur. *Arabian J. Chem.*, **5**, 201 (2012).

[33] C. Jayabalakrishnan, K. Natarajan. *Synth. React. Inorg. Met.-Org. Chem.*, **31**, 983 (2001).

[34] P.M. Vimal Kumar, P.K. Radhakrishnan. Inorg. Chim. Acta, **375**, 84 (2011).

[35] H.-Zh. Ma, B. Wang, Q.-Zh. Shi. *Synth. React. Inorg. Met.-Org. Chem.*, **32**, 617 (2002).

[36] D. Banerjea. *Coordination Chemistry*, Tata McGraw-Hill, New Delhi (1993).

[37] S.F.A. Kettle, *Coordination Compounds*, ELBS, Essex (1969).

[38] M. Hanif, Z.H. Chohan. *Appl. Organomet. Chem.*, **27**, 36 (2013).

[39] N. Raman, K. Pothiraj, T. Baskaran. *J. Coord. Chem.*, **64**, 3900 (2011).

[40] B.J. Hathaway, D.E. Billing. *Coord. Chem. Rev.*, **5**, 143 (1970).

[41] B.J. Hathaway. *Struct. Bond.*, **57**, 55 (1984).

[42] J. Joseph, K. Nagashri, G.B. Janaki. *Eur. J. Med. Chem.*, **49**, 151 (2012).

[43] B.J. Hathaway, G. Wilkinson, R.D. Gillard, J.A. McCleverty (Eds.). *Comprehensive Coordination Chemistry*, Vol. 5, Pergamon, Oxford (1987).

[44] M. Ikram, S. Rehman, M. Ali, C. Faridoon, C. Schulzke, R.J. Baker, A.J. Blake, K. Malook, H. Wong, Saeed-Ur-Rehman. *Thermochim. Acta*, **562**, 22 (2013).

[45] N.V. Kulkarni, V.K. Revankar, B.N. Kirasur, M.H. Hugar. *Med. Chem. Res.*, **21**, 663 (2012).

[46] S. Tabassum, M. Zaki, F. Arjmand, I. Ahmad. *J. Photochem. Photobiol. B*, **114**, 108 (2012).

[47] P. Kavitha, K. Laxma Reddy. *Bioinorg. Chem. Appl.*, **2014**, 1 (2014).

[48] S.A. Patil, V.H. Naik, A.D. Kulkarni, P.S. Badami. *J. Sulfur Chem.*, **31**, 109 (2010).

[49] T.A. Yousef, G.M. Abu El-Reash, O.A. El-Gammal, R.A. Bedier. *J. Mol. Struct.*, **1029**, 149 (2012).

[50] P. Subbaraj, A. Ramu, N. Raman, J. Dharmaraja. *J. Coord. Chem.*, **67**, 2747 (2014).

[51] A. Srishailam, Y.P. Kumar, P. Venkat Reddy, N. Nambigari, U. Vuruputuri, S.S. Singh, S. Satyanarayana. *J. Photochem. Photobiol. B*, **132**, 111 (2014).

[52] R.G. Pearson. *Acc. Chem. Res.*, **26**, 250 (1993).

[53] R.G. Pearson. *Hard and Soft acids and bases*, Dowden, Hutchinson and Ross, Stroudsburg, PA (1973).